Plasma-induced non-equilibrium electrochemistry synthesis of nanoparticles for solar thermal energy harvesting

Ruairi McGlynn[a], Supriya Chakrabarti[a], Bruno Alessi[a], Hussein S. Moghaieb[a], Paul Maguire[a], Harjit Singh[b], Davide Mariotti[a,*]

[a] *Nanotechnology and Integrated Bio-Engineering Centre (NIBEC), Ulster University, Newtownabbey BT37 0QB, United Kingdom*
[b] *Institute of Energy Futures, Brunel University London, Uxbridge UB8 3PH, United Kingdom*

ARTICLE INFO

ABSTRACT

Rapid plasma-induced non-equilibrium electrochemistry (PiNE) at atmospheric pressure was used to prepare surfactant-free gold nanoparticles and copper oxide quantum dots. A suite of chemical and physical characterisation is carried out to assess the as-prepared materials. Nanofluids comprised of these nanoparticles in ethylene glycol have been prepared. The energy absorptive properties of the prepared nanofluids were investigated as a potential additive to the traditional working fluids used in solar thermal collectors. The application feasibility has been assessed by calculating a value of power which could be transferred to the thermal fluid. This work demonstrates an alternative and rapid method to produce nanofluids for solar thermal conversion.

1. Introduction

With a continuing increase in demand for energy and the concomitant environmental pollution caused by the use of fossil fuels for its production, it is essential to obtain as much energy as possible from zero-carbon, renewable sources. Amongst these renewable options, solar energy represents a significant potential source for future energy needs and recently advanced methods of solar energy harvesting have been modelled. Examples include non-equilibrium plasma-assisted solar absorption for the thermochemical decomposition of CO_2 (Elahi et al., 2020) and also concentrated photovoltaics/solar thermoelectric generators/Stirling engine hybrid systems (Mohammadnia et al., 2020), however, simple photoelectrical or photothermal processes are much more common. Alongside photovoltaic cells, solar thermal collectors are the most commonly used solar energy collection devices, converting absorbed solar energy to thermal energy. A typical collector consists of a selectively coated surface to absorb solar radiation, which is transferred to a working fluid in the form of heat by conduction and convection. The solar thermal conversion efficiency of this multi-step process is an issue, as not only does the effectiveness of the heat exchange process between the absorber and the fluid affect the amount of actual heat supplied, but the rate of heat transfer into and out of the fluid also plays a crucial role in the efficiency (Otanicar et al., 2010; Phelan et al., 2013).

As an attempt to reduce heat loss in traditional solar collectors, directly absorbing solar collectors (DASCs) were developed in the 1970s, where the absorption media is the heat transfer fluid (Minardi and Chuang, 1975). In order to overcome the poor absorption in the visible range of typically used working fluids such as water, ethylene glycol (EG) and diathermic oils (Bertocchi et al., 2004; Minardi and Chuang, 1975), additives must be incorporated in the fluid to trap the incident solar energy. With around 90% of the total incident radiation in the visible range transmitted through water and EG (Otanicar et al., 2009), the criticality of altering the fluid properties to absorb this significant portion of incident energy is apparent (ASTM International and ASTM, 2012). μm-sized carbonaceous particles were previously used, yielding improved absorptive properties over the base fluid. Nonetheless, issues arose with the poor stability, clogging of pumping equipment and fouling of the transparent cover which hindered the overall system efficiency and lifetime (Bertocchi et al., 2004; Minardi and Chuang, 1975). As such focus has shifted towards nanoparticle-laden fluids, known as nanofluids, which have been proposed as potential absorbing fluids to improve the absorption across this high energy area of the solar spectra, with significantly reduced pump clogging compared to micron-sized particles (Chen et al., 2016a; Otanicar et al., 2009; Tyagi et al., 2009; Wang and Mujumdar, 2007).

It is well known that the optical properties of nanoparticles, such as scattering and absorption, can be tailored through careful selection of

---

nanoparticle material, shapes, size and concentrations (Khlebtsov et al., 2005). The plasmonic resonance peak of metallic gold nanoparticles (Au NPs) in particular, is a well-documented phenomenon which can greatly enhance scattering and absorption of incident light (Beicker et al., 2018; Chen et al., 2016a; Link and El-Sayed, 2000, 1999; Patel et al., 2013; Sharaf et al., 2019), though many other materials have been investigated such as gold nanorods (Jeon et al., 2016), aluminium (Tyagi et al., 2009), carbon nanotubes (Beicker et al., 2018; Delfani et al., 2016; Karami et al., 2014), carbon nanohorns (Bortolato et al., 2017; Gimeno-Furio et al., 2019), graphene/graphene oxide (Rose et al., 2017; Vakili et al., 2016; Chen et al., 2017), silver (Asmussen and Vallo, 2018; Mallah et al., 2018; Otanicar et al., 2010; Taylor et al., 2011), copper oxide nanoparticles (CuO NPs) (Karami et al., 2016, 2015; Menbari et al., 2016) or other metallic nanoparticles (Amjad et al., 2018; Pustovalov and Astafyeva, 2018), as well as blended or mixed nanomaterials (Mehrali et al., 2018; Qu et al., 2019; Ulset et al., 2018). As such it is possible to produce tailored nanofluids in terms of absorptive properties within the visible light range by careful selection of additive nanomaterials. Whilst it stands to reason that increasing the concentration of nanoparticles would increase the amount of energy harvested, this is not always true, and the concentration must be also carefully selected as both too high and too low a concentration can be detrimental to performance (Beicker et al., 2018; Taylor et al., 2011). This can be attributed to the reduced penetration depth (for the case of too great a concentration) of the incident light due to the added nanoparticles. This trapping of energy in the top few millimetres of the fluid leads to a higher average surface temperature of the receiver, which presents favourable conditions for loss of thermal energy to the surroundings (Hewakuruppu et al., 2015; Khullar et al., 2014; Taylor et al., 2011). Ultimately, this re-emitted energy constitutes a system loss and results in a less efficient nanofluid.

Au NPs are a well-studied material, with a size-tunable plasmonic absorption peak in the visible region of the spectra (Beicker et al., 2018; Chen et al., 2016a; Link and El-Sayed, 2000, 1999; Patel et al., 2013; Sharaf et al., 2019) and good chemical stability (Patel et al., 2013), and as such lend themselves as a model material to add to our nanofluids. Whilst gold is a costly material, the plasmonic absorption effect is of such magnitude that even at a very low concentration of Au NPs a significant attenuation of visible light between 520 nm and 580 nm can be achieved (Haiss et al., 2007). Many works have focused on producing Au NPs with a very narrow size distribution (± 5 nm) (Lu et al., 2008; Steinigeweg et al., 2011; Suchomel et al., 2018), often requiring time-consuming post-processing steps, which results in dispersions that absorb very strongly in a very narrow range. For this application it is vital to absorb as many of the high energy photons in the visible light region as possible, and as such a narrow size distribution may hinder the applicability. To this end, a larger size distribution is acceptable, even beneficial. As such an extremely rapid PiNE system can be used to rapidly fully reduce gold salts, synthesising surfactant-free Au NPs within 10 min.

In addition, CuO quantum dots (QDs) are investigated as a complementary additive to Au NPs as these particles have been demonstrated to greatly increase the attenuation of light (up to four-fold) at the shorter wavelength end of the visible region into the UV region (Karami et al., 2016, 2015; Velusamy et al., 2017). Furthermore, these particles can be created at very low cost from a copper foil submerged in ethanol and exposed to a cathodic microplasma discharge of only a few Watts of power. These nanoparticles have been shown to be very small, with a small size distribution (Velusamy et al., 2017) as well as remaining stable for a period of over 1 year.

Herein we report the synthesis of surfactant-free Au NPs and CuO QDs by PiNE. The produced particles are physically and chemically characterised by a suite of techniques. These particles are then dispersed into ethylene glycol and the optical properties are assessed. Finally, the stability of the nanofluid over a period of 11 weeks is assessed.

2. Methods

2.1. Gold nanoparticle synthesis

The synthesis of the Au NPs was performed on the basis of the work by Patel *et al.* (Patel et al., 2013). Briefly, Au NPs were synthesized by PiNE where a plasma was generated above the surface of an aqueous solution with various concentrations of $HAuCl_4$ (Fig. 1a). The process yields Au NPs within a few minutes, with the concentration of particles increasing with the processing time until the precursor salt is depleted. In the previous work (Patel et al., 2013) it was found that the absorbance peak of the synthesised Au NPs was greatest at a salt concentration of 0.6 mM. As such a stock solution of 6 mM $HAuCl_4$ in 15 $M\Omega$ cm^{-1} deionised water was prepared and mixed with additional deionised water to produce an electrolyte of 0.6 mM for processing. No other reagents, such as reducing agents or surfactants were added to this gold stock solution, and all glassware was cleaned with aqua regia solution prior to usage. A direct current (DC) powered helium microplasma was generated across a gap of 1 mm between a nickel capillary tube (inner diameter of 0.7 mm and an outer diameter of 1 mm) and the surface of a 10 mL aqueous solution of gold (III) chloride trihydrate ($HAuCl_4 \cdot 3H_2O$). The helium gas flow of 25 sccm (controlled by a mass flow controller, MKS Instruments, UK) ensures that the plasma is largely formed in helium gas, although a degree of turbulent mixing is expected with the surrounding air. The power supply (Matsusada AU-10*15) delivers an initial voltage of 900 V, which was applied to a carbon rod (5 mm diameter) submerged in the solution ~1 cm away from the capillary to complete the circuit and allow generation of a microscale discharge. All samples of Au NPs were synthesized at a constant current of 5 mA and for 10 min, with the applied voltage dropping during the process as the solution became more conductive. During synthesis, the solution is seen to change colour from pale yellow to a red/purple as the salt is reduced and Au NPs form. This colour change can be measured by ultraviolet–visible spectroscopy (UV–Vis) as a peak in the red/purple portion of the visible light range and was consistently used to verify the production of Au NPs throughout the study and for the quick screening of a larger number of samples by ensuring the optical characteristics were reproduced accurately.

2.2. Copper oxide nanoparticle synthesis

The synthesis of CuO QDs was carried out on the basis of previous work (Velusamy et al., 2017) where the synthesis mechanisms have been discussed in more details. This is also based on a PiNE process
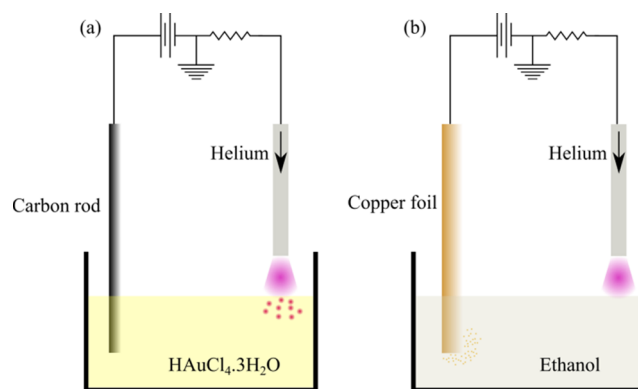

Fig. 1. (a) A diagram of the experimental setup used for the synthesis of nanoparticles. The carbon anode was submerged in dilute gold salt with the nickel capillary tube positioned approximately 1 cm away and maintained 1 mm above the solution surface. (b) A schematic of the experimental setup used for the synthesis of copper oxide quantum dots. A copper foil is submerged into ethanol and is used as the anode, with the cathode of a helium plasma discharge completing the DC circuit.

which uses a plasma generated at the surface of an ethanol solution. A 0.1 mm thick, 1 cm wide sacrificial copper electrode is used and immersed in the solution where QDs are synthesized. This ribbon was then submerged in 5 mL of ethanol in a Pyrex cylinder and acted as the anode. The cathode, in this case, was the helium gas discharge from a nickel capillary (50 sccm). This is shown schematically in Fig. 1b. Initially, the voltage read 3 kV with less than 0.05 mA of current, with the current rising as the solution conductivity increases. After reaching 0.5 mA, the voltage was reduced to maintain a constant current for the remainder of the discharge; this is controlled by the power supply, which enters constant current mode once the set current is reached. The solution was processed for a total of 30 min, with interruptions every 10 min to allow for ethanol vapour to disperse, with additional ethanol being added, refilling the cylinder to its volume before processing.

2.3. Preparation of the nanofluids

2.3.1. Weighing the nanomaterials

Photographs were taken during the steps to prepare the nanofluids and are shown in Fig. 2. In Fig. 2a, four vials with 10 mL of processed 0.6 mM salt solution are shown as prepared. Likewise, in Fig. 2b, five vials of CuO sol are presented as-synthesized. The samples were dried in pre-weighed glass containers placed on top of a hotplate set to 75 °C (Stuart, Hotplate Stirrer SB162-3). A total of 100 mL of Au NP and 50 mL of CuO were dried in sample containers separately. As the solvents for the Au NP and CuO QD sols are water and ethanol respectively, they evaporated at a different rate, with the ethanol evaporating more rapidly. As soon as the solvent is evaporated, the vial was removed from the hot plate. This heating process took approximately 3 h for the CuO QD vial and 8 h for the Au NP sols. While Au NPs have

shown to be stable after synthesis, it was observed that Au NPs settled to the bottom of the vial during heating within several hours as can be seen in Fig. 2c (left). The CuO sols do not appear to settle to the same degree as the Au NP sols, but there is a small amount of material settling out of the solution. This could imply that they are agglomerating and hence falling out of suspension (Fig. 2c, right). The mass of the dried material was measured again, allowing for the determination of the mass of the sample (see Supporting Information) and thus the volume. Both materials form a dry powder-like coating on the base of the glass container as can be seen in Fig. 2d. The equation $V = \frac{m}{\rho}$ was used to calculate the volume of the additive particles, where V is the volume, m is the mass and ρ is the density. Using the values of 19.32 g cm^{-3} for Au and 6.315 g cm^{-3} for CuO volumes of 0.55 µL and 0.17 µL were determined for the Au and CuO particles respectively (National Center for Biotechnology Information, 2018a, 2018b).

2.3.2. Mixing the nanofluid

The 10 mL of EG was added to the dried material and a vol:vol percentage was calculated. The same process was followed for forming the blended nanofluids, where the volume of both additives was calculated from mass and density and added to 10 mL of EG to form sols with vol:vol percentages of each component (see Supporting Information). The vials containing 10 mL of EG and the dried material were then vortexed at 1000 revolutions per minute (RPM) for 1 min (Fisher scientific, TopMIX FB15013), yielding the nanofluids in Fig. 2e. From Fig. 2f it can be seen that whilst most of the dried particles can be redispersed into EG to form nanofluids, some dried mass is seen on the base of the vials, which constitutes a loss of NP in the process.
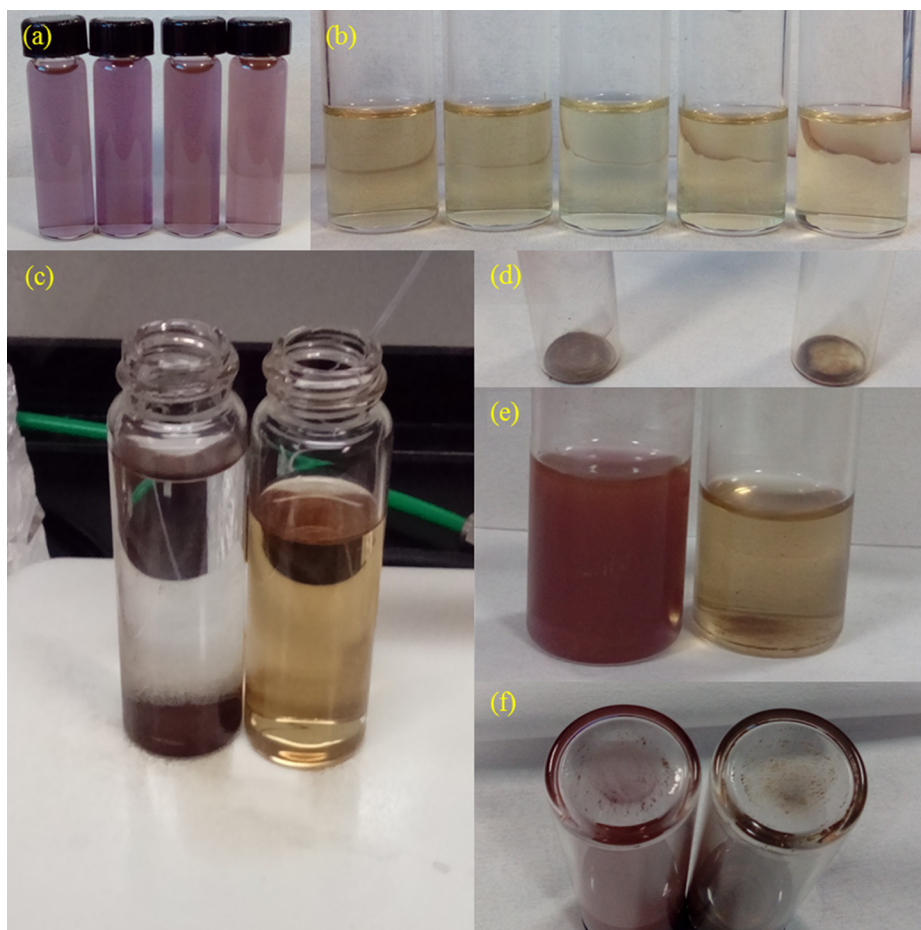

Fig. 2. Photographs of the different stages of nanofluid preparation. Images (a) and (b) show the gold and copper oxide solutions formed in the PiNE system as-synthesised. Image (c) shows the cylinders on a hotplate taken after 1 h of heating. Image (d) shows resultant dry mass after full evaporation of the solvent. Image (e) shows the resultant sols when ethylene glycol is added to the cylinders containing dry mass and vortexed. From an image (f) it is clear some dry material remains adhered to the bottom of the cylinder after vortexing.
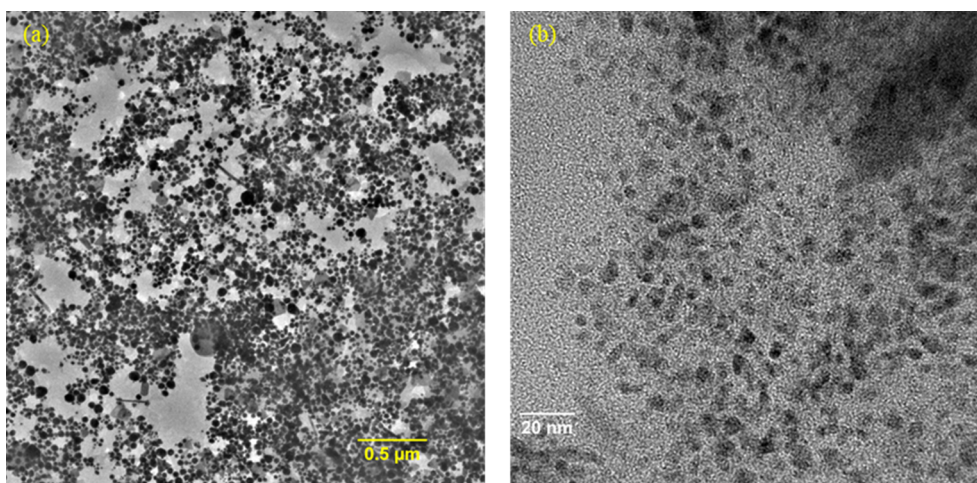
Fig. 3. Representative TEM images of (a) as-prepared Au NP sample and (b) CuO QDs.

3. Results and discussion

3.1. Nanoparticle characterization

To assess our as-prepared materials we have employed a suite of characterisation equipment, utilising X-ray photoelectron spectroscopy (XPS), X-ray diffraction (XRD) and transmission electron microscopy (TEM) analysis, including selective area electron diffraction (SAED).

The as-made Au NP dispersion contains a range of shapes and sizes (Fig. 3a), with the majority of particles consisting of small spherical nanoparticles, however, some nanorods and larger triangular particles were observed. In order to measure the size of different shapes of NPs we considered the size of rods as that of the longest dimension and the size of triangular particles was considered as the largest distance from the tip to the opposite side (see Supporting Information). When the particle size is assessed inclusive of all the different shapes a mean particle size of 27 nm is obtained from a log-normal fitting (see Supporting Information). The CuO particles are found to have a mean particle size of 3.3 nm, to be nearly spherical and with little to no agglomeration (Fig. 3b and Supporting Information). The mean diameter was determined by TEM imaging of ~300 particles and fitted with a log-normal distribution. As the Bohr exciton radius for CuO is expected to lie between 6.6 nm and 28.7 nm (Borgohain and Mahamuni, 2002), the CuO particles produced in this work are expected to fall within the strong quantum confinement regime and are therefore referred to herein as QDs. This mean size of 3.3 nm is slightly larger than the mean size of 1.9 nm in our previous work (Velusamy et al., 2017) and can be attributed to the change in the electrode spacing in the present work. It has been observed that reducing the electrode spacing from 3 cm to 1 cm (this work) the time required to reach the set current of 0.5 mA is reduced. This has the effect of enhancing the absorbance of the CuO dispersion formed for a given treatment time as seen in Fig. 4, and is likely the cause of the increased particle size.

The crystallinity of the produced materials was verified with XRD and SAED measurements (Fig. 5 and Supporting Information). For the Au NP samples (Fig. 5a), both of these techniques show five features which could be assigned based on face-centered cubic gold, the {1 1 1} plane appears to be predominant, with four other peaks appearing corresponding to the {2 0 0}, {2 2 0}, {3 1 1} and {2 2 2} planes (Biao et al., 2018; Kumar et al., 2014; Verma et al., 2010). For the CuO QDs, the XRD diffractogram (Fig. 5b) can be fit on the basis of monoclinic CuO in accordance with JCPDF 89-5896. A total of 10 peaks can be fitted and amongst these several match the Miller indices obtained from the electron diffraction pattern. Several of these planes can be observed in the SAED, notably, {−1 1 1}, {2 0 2} and {2 2 0}, which corroborates that we have produced monoclinic CuO.

The chemical state of the produced particles was assessed by XPS, presented in Fig. 6. To confirm the reduction of the gold salt a sample of the untreated salt is also compared with the spectrum of the Au NPs sample (Fig. 6a). It is this Au 4f region that is of significant interest in the analysis as deconvolution of this region can elucidate any presence of Au^{3+} or Au^+ ions within the sample, which would suggest that the Au salt is not fully reduced. For the Au NPs sample only two peaks could be fitted in the spectra, Au $4f_{5/2}$ at 87.76 eV and Au $4f_{7/2}$ at 84.09 eV, which correspond to metallic Au^0 and indicate that the treatment by microplasma is capable of fully reducing the $HAuCl_4$ precursor (Anthony and Seah, 1984; Turner and Single, 1990). The spectra of the untreated sample exhibit two peaks shifted to the higher binding energy (84.5 e.V and 88.2 eV), suggesting the oxidation state of Au^+ (Abad et al., 2005; Corma and Garcia, 2008). Whilst the expected oxidation state of Au in $HAuCl_4$ is Au^{3+}, the photoreduction of Au^{3+} to the lower oxidation state of Au^+ by the XPS instrument (Abad et al., 2005) could result in the absence of Au^{3+} in the untreated salt sample. Regardless, it is clear that no peak can be attributed to the Au^0 state with the untreated salt sample and the Au NPs sample does not show any unreduced or partially reduced Au; as such a clear distinction can be made between the salt sample and the plasma-treated sample. The Cu 2p narrow region spectra for the CuO QDs is presented in Fig. 6b, which shows a strong peak at 933.2 eV which is a typical position for Cu^{2+}. This peak is shifted by at least 0.5 eV from the peak centres expected for either metallic Cu^0 (932.6 eV) or Cu^+ (932.7 eV) and thus these two states are not present in the sample. In addition to the main Cu^{2+} peak, two shake-up satellites appear at 940.9 eV and 943.4 eV which are characteristic of CuO and do not appear strongly for Cu_2O or at all for Cu^0 (Hassanien et al., 2016; Hernández et al., 2007; Jiang et al., 2013; Wang et al., 2015). Therefore, we have confirmed that the material produced is Copper (II) oxide.

3.2. Optical properties of the nanofluid

Within a nanofluid, incident power from solar radiation can interact in two ways in addition to being transmitted with no interaction; firstly, the radiation can be absorbed by the fluid or the NP additive. Alternatively, the light may be scattered by the NPs, which results in either the light scattering out of the fluid body and subsequently being lost from the system, or in light being absorbed in the scattered path. The absorption coefficient is of great interest to this work and has been calculated from the UV–Vis data (see Supporting Information) and illustrates how a collimated beam of light is attenuated due to absorption by the sample within a given path length. Likewise, the scattering coefficient is calculated in order to assess the attenuation due to scattering of light by the nanofluid. A number of nanofluids with Au NPs
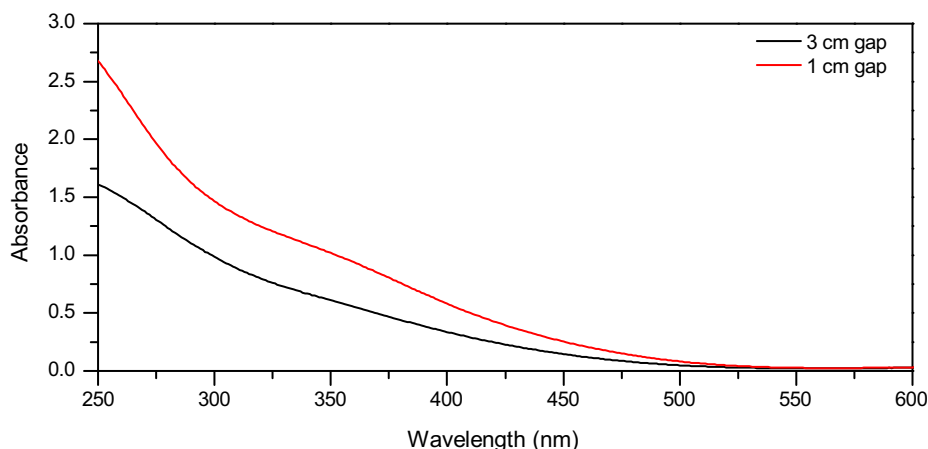
Fig. 4. The ultraviolet–visible spectra of copper oxide dispersions formed in ethanol when the gap between the electrodes is reduced from 3 cm (black line) to 1 cm (red line). (For interpretation of the references to colour in this figure legend, the reader is referred to the web version of this article.)

only (volume:volume percentages of $2.2 \times 10^{-3}\%$, $3.3 \times 10^{-3}\%$ and $5.5 \times 10^{-3}\%$), with CuO QDs only (of $0.7 \times 10^{-3}\%$, $1.0 \times 10^{-3}\%$ and $1.7 \times 10^{-3}\%$) and with mixed Au NP & CuO QDs ($5.1 \times 10^{-3}\%$ Au NPs and $2.0 \times 10^{-3}\%$ CuO QDs) have been considered and the corresponding absorption and scattering coefficients are reported in Fig. 7.

The concentrations of NPs/QDs has given the expected behaviour with increasing coefficient values for higher volume concentrations of the same nanofluid (Fig. 7). It is noted that the Au NPs nanofluid presents an absorption coefficient dominated by the plasmonic absorption between 540 nm and 560 nm (Fig. 7a, red curves) that is well above the corresponding scattering coefficient (Fig. 7b, red curves) for most of the spectral range. Contrarily, nanofluids with CuO QDs exhibit scattering and absorption coefficients that are comparable throughout (blue curves in Fig. 7a-b). The multicomponent nanofluid also presents interesting features and it can outperform single component nanofluids

for a limited spectral range. Below 588 nm, the blended nanofluid seems to benefit from the simultaneous presence of both Au NPs and CuO QDs while the opposite is observed above 588 nm. This result shows that both positive and negative synergies can occur for blended nanofluids and that understanding the combined mechanisms is not a simple additive process. The reason for high absorption (< 588 nm) can be attributed to a degree of complementarity between Au NPs and CuO QDs absorption coefficients, where the plasmonic absorption peak of the Au NPs is still dominant; however, above ~588 nm, the combined scattering of Au NPs and CuO QDs is clearly attenuating the light to a level that is negatively impacting absorption. It is not coincidental that the absorption coefficient of the blended nanofluid becomes lower than that of Au NPs-only nanofluid within the same wavelength range (see where the green curve crossovers with the full red curve at ~590 nm in Fig. 7a) where the scattering coefficient of CuO QDs becomes stronger
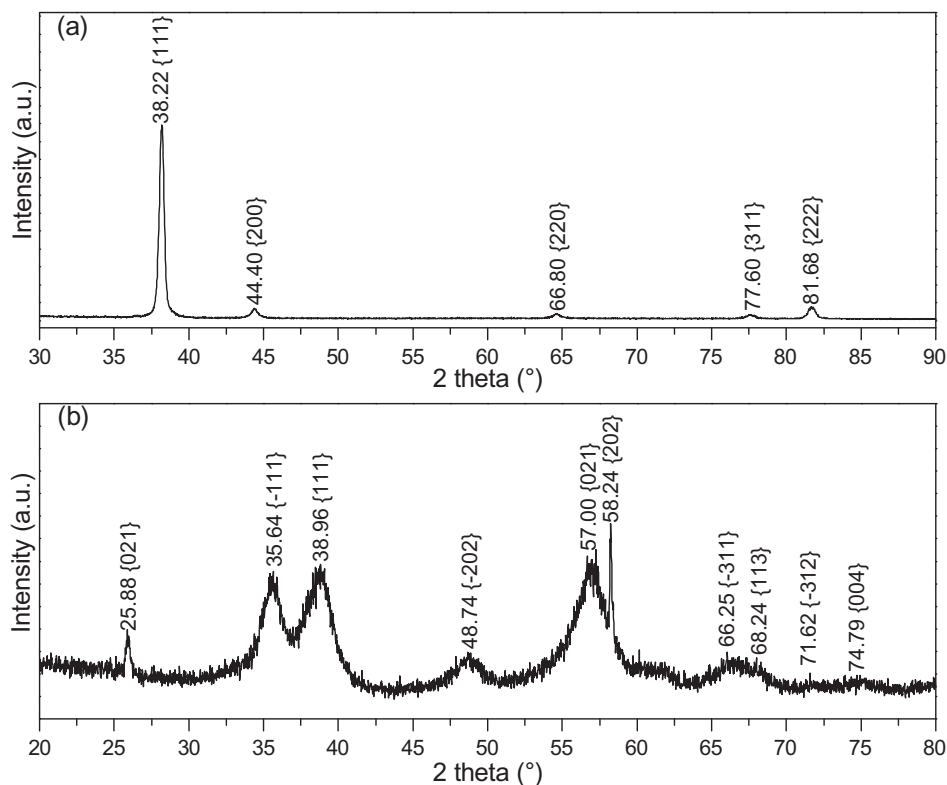

Fig. 5. X-ray diffractograms for the as-prepared nanoparticles, (a) Au NPs sample and (b) CuO QDs.
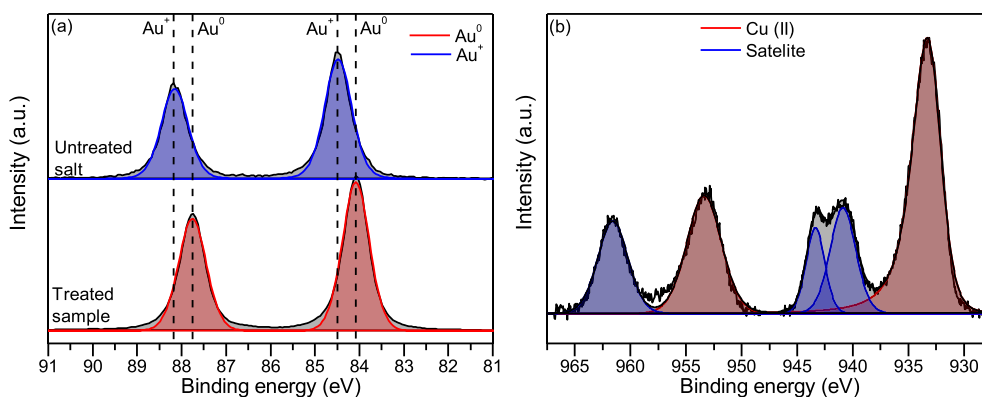
Fig. 6. XPS analysis of the as-prepared particles (a) The Au 4f region of the x-ray photoelectron spectra for Au NPs sample and (b) shows the Cu 2p region for the synthesised CuO QDs.
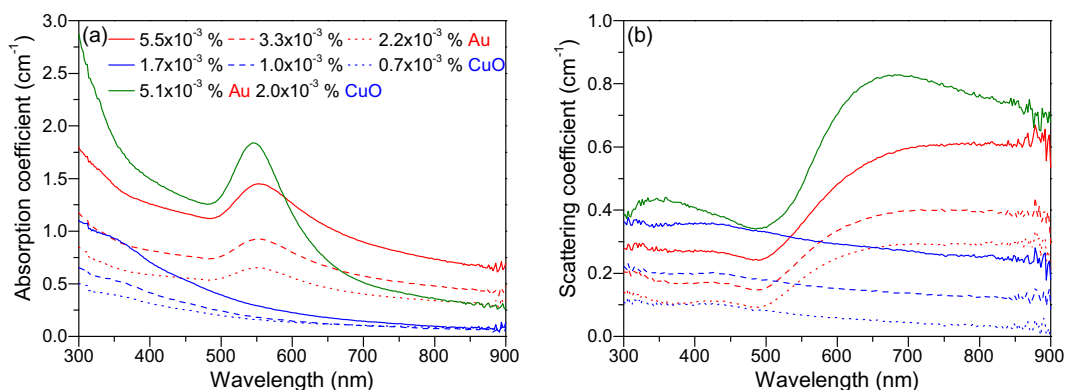

Fig. 7. Calculated estimates of the absorption coefficient (a) and scattering coefficient (b) for a range of different concentrations of gold (red), copper oxide (blue), and gold-copper oxide (green) additives in an ethylene glycol base fluid. (For interpretation of the references to colour in this figure legend, the reader is referred to the web version of this article.)

than its absorption coefficient (~588 nm); for instance, compare $1.7 \times 10^{-3}\%$ CuO QDs (full blue curves) in Fig. 7a and b and note that the absorption coefficient decreases to 0.2 cm^{-1} just below 600 nm.

On the basis of the nanofluid physical parameters, we will now calculate the absorbed power for different fluid depth under solar irradiation (see Supporting Information). While a fraction of scattered light in the nanofluid can be re-absorbed, in our calculations we have considered scattering as a loss and therefore our results provide a lower bound to the absorbed power. Fig. 8 reports the calculated absorbed power for the different nanofluid concentrations and for varying fluid depth. We report these results both in absolute values of power per surface area (Fig. 8a) as well as a percentage of the total irradiated

power (Fig. 8b). For the Au NP nanofluids, a small increase in the fluid depth from 0.1 cm to 1 cm gives a dramatic increase in power absorbed to over 300 W m^{-2}, with higher volume concentrations giving a greater power absorbed for a given fluid depth (Fig. 8a). Beyond this depth, tending towards 3 cm, the increase of absorbed power with fluid depth begins to plateau. This can be considered an effect of the high absorption and scattering coefficients observed for the Au NPs nanofluids which result in very large portions of incident radiation being attenuated at small fluid depth. Fig. 8b, however, shows that the nanofluid is not able to absorb all the solar power available, the reason is attributed to the strong scattering coefficient at longer wavelengths, which will always ensure that a fraction of the incident light escapes the
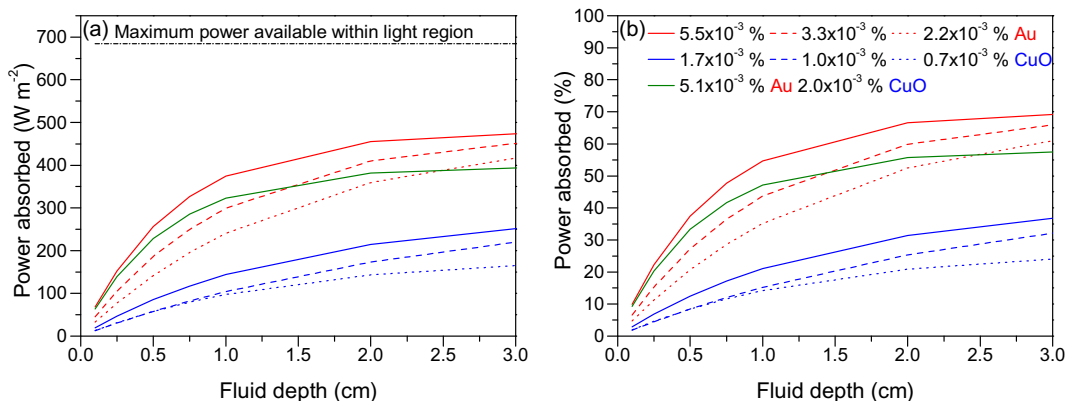

Fig. 8. The calculated power absorbed by nanofluids is determined for lengths scales ranging from 0.1 cm to 3 cm. (a) Power absorbed per m^2 is plotted from the solar irradiance spectra between 300 and 900 nm. (b) The percentage of power absorbed per m^2 was determined and charted.

nanofluid. A similar trend can be observed for the CuO nanofluids, with an increase in power absorption between 0.1 cm and 3 cm, albeit less rapid, and higher volume concentration nanofluids absorbing more power. The performance of CuO as a nanofluid additive in the calculations appears to be inferior to that of Au NPs, where, even for comparable concentrations (2.2×10^{-3}% Au NPs and 1.7×10^{-3}% CuO QDs), the Au NP nanofluid absorbs more than double that of the CuO nanofluid. Interestingly, the blended nanofluid of 5.1×10^{-3}% Au NPs and 2.0×10^{-3}% CuO QDs is outperformed by the nanofluid consisting of 5.5×10^{-3}% Au NPs alone. As an example, at a fluid depth of 1.5 cm, the blended nanofluid can absorb ~50% of the incident power (Fig. 8b), whilst the 5.5×10^{-3}% Au NP nanofluid can harvest close to 60%. The performance of the multi-component nanofluid in Fig. 8 is the outcome of competing mechanisms, which have shown to benefit absorption at lower wavelengths (< 588 nm) but are counterproductive at longer wavelengths as per our discussion of Fig. 7. Our calculations of absorbed power indicate that, overall, the negative impact of the scattering phenomena introduced by the CuO QDs are significant to the point that nanofluid with Au NPs only are preferable.

3.3. Nanofluid stability

The ability of a nanofluid to retain its absorptive properties throughout its working life is paramount to its industrial uptake. As such the stability of the prepared nanofluids, in terms of power absorption capability, was assessed over time for the CuO QDs and Au NPs nanofluids with the highest concentrations as well as for the nanofluid with blended NPs. The samples were stored in a dark cupboard and were not shaken, sonicated, vortexed or otherwise disturbed during the storage period of 11 weeks. The stability of each of the nanofluids was investigated by re-measuring the optical properties of the samples after a few seconds of shaking and calculating the potential to absorb power. A reduction in the absorption coefficient for each nanofluid is seen in Fig. 9a, with the decrease in absorption coefficient most severe for the CuO nanofluid and blended nanofluid, with a very slight decrease for the Au nanofluid. This would suggest that some of the NPs and/or QDs may have agglomerated and sedimented to the point where they are no longer active in absorbing incident power. In Fig. 9b the scattering coefficient is observed to remain constant for the Au NPs nanofluid and increases substantially for the CuO QDs nanofluid. Interestingly, the scattering coefficient is seen to decrease in the case of the blended nanofluid. Whilst the behaviour of the Au NPs nanofluid and the blended nanofluid are expected with a stable nanofluid and one where some material is sedimenting, the behaviour of the CuO nanofluid is more complex as the scattering coefficient is larger after 11 weeks. The increase of the scattering component can possibly be explained through the equations for the scattered light intensity by Rayleigh scattering Eq. (1) (Seinfeld and Pandis, 2006).
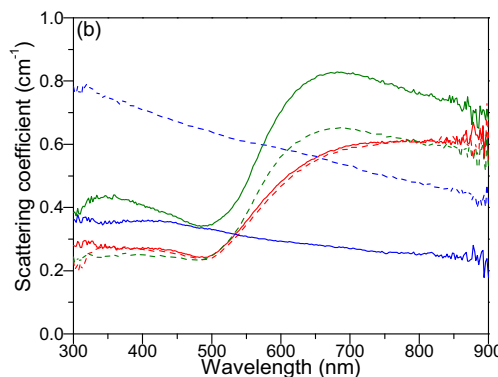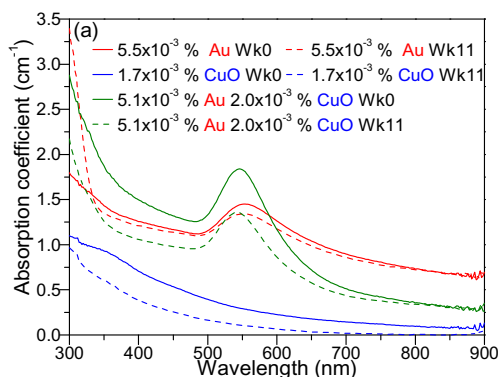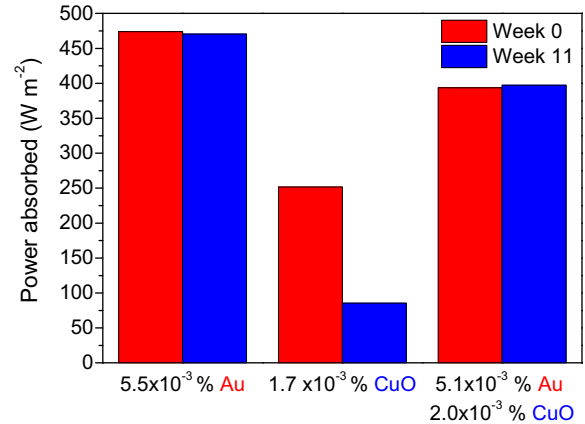

Fig. 10. The stability of nanofluid was assessed after 11 weeks with both the gold and the gold-copper oxide nanofluids retaining their affinity for power absorption for a fluid depth of 3 cm. A decrease in power absorption for the copper oxide alone sample is observed.

$$I_S = I_0 \left(\frac{1 + \cos^2 \theta}{2R^2} \right) \left(\frac{2\pi}{\lambda} \right)^4 \left(\frac{n^2 - 1}{n^2 + 2} \right)^2 \left(\frac{d}{2} \right)^6 \tag{1}$$

$$Q_{S\lambda} = \frac{8}{3}\alpha^4 \left[\left(\frac{m^2 - 1}{m^2 + 2} \right) \right]^2 \tag{2}$$

where I_S is the intensity of scattered light, I_0 is the intensity of incident light, R is the distance from the source to the particle, θ is the scattering angle, λ is the wavelength, n is the refractive index of unpolarised light, d is the diameter of a spherical particle, α is the size parameter and m is the complex refractive index. This equation highlights the sixth power relationship between the diameter d of a sphere and the scattered light intensity I_S. Additionally, the scattering efficiency, $Q_{S\lambda}$, is known to be linked to the fourth power of the nanoparticle size α parameter, equation (2) (Chen et al., 2016b; Saidur et al., 2012; Taylor et al., 2011). Therefore, if the CuO QDs were to grow even slightly by agglomeration, this enhanced scattering could be accounted for.

We now considered the effect of time on absorbed power and compare the power absorbed by a nanofluid of 3 cm depth over the 11-week period considered earlier (Fig. 10). Whilst the CuO QDs nanofluid absorbed power has diminished, both the Au NPs and blended nanofluids are able to retain their absorptive properties over the 11 weeks of storage. This is of course very interesting in terms of a DASCs as it suggests that these surfactant-free Au NPs could maintain high absorptive properties over extended periods of operation, with no additional mixing required beyond that of the pumping system. This stability will result in lower maintenance costs, making the solution much more economically attractive. It is interesting to note that in this specific case, the performance degradation of the CuO QDs is not affecting that of the blended nanofluid, which indicates no detrimental physical

Fig. 9. Calculated estimates of the absorption and scattering coefficients for a range of different concentration of gold (red), copper oxide (blue), and gold-copper oxide (green) nanofluids. (a) Absorption coefficient. (b) Scattering coefficient. (For interpretation of the references to colour in this figure legend, the reader is referred to the web version of this article.)

interactions between Au NPs and CuO QDs. While this specific combination of absorber-scatterer could outperform single component nanofluid only in a limited spectral range, a more careful selection of NPs with more complementary properties could bring greater benefits.

4. Conclusion

Au NPs and CuO QDs nanofluids have been produced by PiNE. The produced nanofluids are capable of increasing the amount of energy captured from the incident light on a solar thermal collector by the fluid when compared to the EG base fluid alone, with larger particle concentrations yielding greater absorption. A strong plasmonic absorption centred between 540 nm and 560 nm is present for the Au NP nanofluid, which when coupled with the strong scattering coefficient at longer wavelengths leads to a large fraction of the incident light escaping the nanofluid for a given length. However, as the absorption coefficient is much larger than the scattering coefficient a significant proportion of the attenuated photons is absorbed by the nanofluid. The performance of CuO as a nanofluid additive in the calculations (where scattering is considered a system loss) is demonstrably lower than that of Au NPs, where even for comparable concentrations, the Au NP nanofluid absorbs more than double that of the CuO nanofluid and can be attributed to the comparable scattering and absorption coefficients of the CuO nanofluid. Interestingly, the blended nanofluid is outperformed by the nanofluid consisting of a comparable concentration of Au NPs alone. As an example, at a fluid depth of 1.5 cm, an additional 10% of the incident power can be absorbed by the Au NP only nanofluid. However, the blended nanofluid possesses superior absorption in the < 588 nm region which highlights a degree of complementarity between the two additives materials. Contrarily, at wavelengths longer than ~588 nm, the combined scattering of Au NPs and CuO QDs is attenuating the light to a level that is negatively impacting absorption.

The stability of the dispersions was tested after storage for 11 weeks, with the Au NP and the blended nanofluid retaining their full absorptive capabilities. The CuO-based nanofluid only managed to retain approximately one-third of its power absorption capabilities. This serves to highlight that a nanofluid based on Au NP is a viable option for DASC application. While these CuO-nanofluids or a mixture of the two particle types did not produce better results than Au NPs nanofluid, there is scope to investigate combinations of "optically complementary" NPs in blended nanofluids. Importantly the full understanding of optical interactions among different NPs in nanofluid is more complex than a simple additive process.

The PiNE system used in this work has been demonstrated to be highly suitable for producing additives for nanofluids with attractive optical properties. The flexibility of reagents in the PiNE system can further facilitate a range of alternative additives such as titanium-based NPs or other plasmonic silver NPs, with no additional equipment requirements.

Acknowledgements

Appendix A. Supplementary material

Supplementary data to this article can be found online at https://doi.org/10.1016/j.solener.2020.04.004.

References

Abad, A., Concepción, P., Corma, A., García, H., 2005. A Collaborative Effect between Gold and a Support Induces the Selective Oxidation of Alcohols. Angew. Chemie Int. Ed. 44, 4066–4069. https://doi.org/10.1002/anie.200500382.

Amjad, M., Jin, H., Du, X., Wen, D., 2018. Experimental photothermal performance of nanofluids under concentrated solar flux. Sol. Energy Mater. Sol. Cells 182, 255–262. https://doi.org/10.1016/j.solmat.2018.03.044.

Anthony, M.T., Seah, M.P., 1984. XPS: Energy calibration of electron spectrometers. 2—Results of an interlaboratory comparison. Surf. Interface Anal. 6, 107–115. https://doi.org/10.1002/sia.740060303.

Asmussen, S.V., Vallo, C.I., 2018. Absorber materials based on polymer nanocomposites containing silver nanoparticles for solar thermal collectors. Sol. Energy 174, 640–647. https://doi.org/10.1016/j.solener.2018.09.062.

ASTM International, ASTM, 2012. Standard Tables for Reference Solar Spectral Irradiances: Direct Normal and Hemispherical on 37° Tilted Surface. https://doi.org/10.1520/G0173-03R12.

Beicker, C.L.L., Amjad, M., Bandarra Filho, E.P., Wen, D., 2018. Experimental study of photothermal conversion using gold/water and MWCNT/water nanofluids. Sol. Energy Mater. Sol. Cells 188, 51–65. https://doi.org/10.1016/j.solmat.2018.08.013.

Bertocchi, R., Karni, J., Kribus, A., 2004. Experimental evaluation of a non-isothermal high temperature solar particle receiver. Energy 29, 687–700. https://doi.org/10.1016/j.energy.2003.07.001.

Biao, L., Tan, S., Meng, Q., Gao, J., Zhang, X., Liu, Z., Fu, Y., 2018. Green Synthesis, Characterization and Application of Proanthocyanidins-Functionalized Gold Nanoparticles. Nanomaterials 8, 53. https://doi.org/10.3390/nano8010053.

Borgohain, K., Mahamuni, S., 2002. Formation of Single-phase CuO Quantum Particles. J. Mater. Res. 17, 1220–1223. https://doi.org/10.1557/JMR.2002.0180.

Bortolato, M., Dugaria, S., Agresti, F., Barison, S., Fedele, L., Sani, E., Del Col, D., 2017. Investigation of a single wall carbon nanohorn-based nanofluid in a full-scale direct absorption parabolic trough solar collector. Energy Convers. Manage. 150, 693–703. https://doi.org/10.1016/j.enconman.2017.08.044.

Chen, L., Xu, C., Liu, J., Fang, X., Zhang, Z., 2017. Optical absorption property and photothermal conversion performance of graphene oxide/water nanofluids with excellent dispersion stability. Sol. Energy 148, 17–24. https://doi.org/10.1016/j.solener.2017.03.073.

Chen, M., He, Y., Zhu, J., Kim, D.R., 2016a. Enhancement of photo-thermal conversion using gold nanofluids with different particle sizes. Energy Convers. Manage. 112, 21–30. https://doi.org/10.1016/j.enconman.2016.01.009.

Chen, M., He, Y., Zhu, J., Wen, D., 2016b. Investigating the collector efficiency of silver nanofluids based direct absorption solar collectors. Appl. Energy 181, 65–74. https://doi.org/10.1016/j.apenergy.2016.08.054.

Corma, A., Garcia, H., 2008. Supported gold nanoparticles as catalysts for organic reactions. Chem. Soc. Rev. 37, 2096. https://doi.org/10.1039/b707314n.

Delfani, S., Karami, M., Behabadi, M.A.A.-, 2016. Performance characteristics of a residential-type direct absorption solar collector using MWCNT nanofluid. Renew. Energy 87, 754–764. https://doi.org/10.1016/j.renene.2015.11.004.

Elahi, R., Nagassou, D., Mohsenian, S., Trelles, J.P., 2020. Enhanced solar radiation absorption by carbon dioxide in thermodynamic nonequilibrium: A computational study. Sol. Energy 195, 369–381. https://doi.org/10.1016/j.solener.2019.11.015.

Gimeno-Furio, A., Hernandez, L., Barison, S., Agresti, F., Cabaleiro, D., Mancin, S., 2019. Optical characterisation of oxidised carbon nanohorn nanofluids for direct solar energy absorption applications. Sol. Energy 191, 323–331. https://doi.org/10.1016/j.solener.2019.09.012.

Haiss, W., Thanh, N.T.K., Aveyard, J., Fernig, D.G., 2007. Determination of Size and Concentration of Gold Nanoparticles from UV−Vis Spectra. Anal. Chem. 79, 4215–4221. https://doi.org/10.1021/ac0702084.

Hassanien, R., Almaky, M.M., Houlton, A., Horrocks, B.R., 2016. Preparation and electrical properties of a copper-conductive polymer hybrid nanostructure. RSC Adv. 6, 99422–99432. https://doi.org/10.1039/C6RA20325F.

Hernández, M.P., Fernández-Bertrán, J.F., Farías, M.H., Díaz, J.A., 2007. Reaction of imidazole in gas phase at very low pressure with Cu foil and Cu oxides studied by X-ray photoelectron spectroscopy. Surf. Interface Anal. 39, 434–437. https://doi.org/10.1002/sia.2528.

Hewakuruppu, Y.L., Taylor, R.A., Tyagi, H., Khullar, V., Otanicar, T., Coulombe, S., Hordy, N., 2015. Limits of selectivity of direct volumetric solar absorption. Sol. Energy 114, 206–216. https://doi.org/10.1016/j.solener.2015.01.043.

Jeon, J., Park, S., Lee, B.J., 2016. Analysis on the performance of a flat-plate volumetric solar collector using blended plasmonic nanofluid. Sol. Energy 132, 247–256. https://doi.org/10.1016/j.solener.2016.03.022.

Jiang, P., Prendergast, D., Borondics, F., Porsgaard, S., Giovanetti, L., Pach, E., Newberg, J., Bluhm, H., Besenbacher, F., Salmeron, M., 2013. Experimental and theoretical investigation of the electronic structure of Cu 2 O and CuO thin films on Cu(110) using x-ray photoelectron and absorption spectroscopy. J. Chem. Phys. 138, 024704. https://doi.org/10.1063/1.4773583.

Karami, M., Akhavan-Bahabadi, M.A., Delfani, S., Raisee, M., 2015. Experimental investigation of CuO nanofluid-based Direct Absorption Solar Collector for residential applications. Renew. Sustain. Energy Rev. 52, 793–801. https://doi.org/10.1016/j.rser.2015.07.131.

Karami, M., Akhavan-Behabadi, M.A., Raisee Dehkordi, M., Delfani, S., 2016. Thermo-optical properties of copper oxide nanofluids for direct absorption of solar radiation. Sol. Energy Mater. Sol. Cells 144, 136–142. https://doi.org/10.1016/j.solmat.2015.08.018.

Karami, M., Akhavan Bahabadi, M.A., Delfani, S., Ghozatloo, A., 2014. A new application of carbon nanotubes nanofluid as working fluid of low-temperature direct absorption solar collector. Sol. Energy Mater. Sol. Cells 121, 114–118. https://doi.org/10.1016/j.solmat.2013.11.004.

Khlebtsov, N.G., Trachuk, L.A., Mel'nikov, A.G., 2005. The effect of the size, shape, and structure of metal nanoparticles on the dependence of their optical properties on the refractive index of a disperse medium. Opt. Spectrosc. 98, 77–83. https://doi.org/10.1134/1.1858043.

Khullar, V., Tyagi, H., Hordy, N., Otanicar, T.P., Hewakuruppu, Y., Modi, P., Taylor, R.A.,

2014. Harvesting solar thermal energy through nanofluid-based volumetric absorption systems. Int. J. Heat Mass Transf. 77, 377–384. https://doi.org/10.1016/j.ijheatmasstransfer.2014.05.023.

Kumar, A., De, A., Saxena, A., Mozumdar, S., 2014. Environmentally benign synthesis of positively charged, ultra-low sized colloidal gold in universal solvent. Adv. Nat. Sci. Nanosci. Nanotechnol. 5, 025017. https://doi.org/10.1088/2043-6262/5/2/025017.

Link, S., El-Sayed, M.A., 2000. Shape and size dependence of radiative, non-radiative and photothermal properties of gold nanocrystals. Int. Rev. Phys. Chem. 19, 409–453. https://doi.org/10.1080/01442350050034180.

Link, S., El-Sayed, M.A., 1999. Size and Temperature Dependence of the Plasmon Absorption of Colloidal Gold Nanoparticles. J. Phys. Chem. B 103, 4212–4217. https://doi.org/10.1021/jp984796o.

Lu, X., Tuan, H.-Y., Korgel, B.A., Xia, Y., 2008. Facile Synthesis of Gold Nanoparticles with Narrow Size Distribution by Using AuCl or AuBr as the Precursor. Chem. - A Eur. J. 14, 1584–1591. https://doi.org/10.1002/chem.200701570.

Mallah, A.R., Kazi, S.N., Zubir, M.N.M., Badarudin, A., 2018. Blended morphologies of plasmonic nanofluids for direct absorption applications. Appl. Energy 229, 505–521. https://doi.org/10.1016/j.apenergy.2018.07.113.

Mehrali, M., Ghatkesar, M.K., Pecnik, R., 2018. Full-spectrum volumetric solar thermal conversion via graphene/silver hybrid plasmonic nanofluids. Appl. Energy 224, 103–115. https://doi.org/10.1016/j.apenergy.2018.04.065.

Menbari, A., Alemrajabi, A.A., Rezaei, A., 2016. Heat transfer analysis and the effect of CuO/Water nanofluid on direct absorption concentrating solar collector. Appl. Therm. Eng. 104, 176–183. https://doi.org/10.1016/j.applthermaleng.2016.05.064.

Minardi, J.E., Chuang, H.N., 1975. Performance of a "black" liquid flat-plate solar collector. Sol. Energy 17, 179–183. https://doi.org/10.1016/0038-092X(75)90057-2.

Mohammadnia, A., Rezania, A., Ziapour, B.M., Sedaghati, F., Rosendahl, L., 2020. Hybrid energy harvesting system to maximize power generation from solar energy. Energy Convers. Manag. 205, 112352. https://doi.org/10.1016/j.enconman.2019.112352.

National Center for Biotechnology Information, 2018a. Gold [WWW Document]. PubChem Compd. Database. URL https://pubchem.ncbi.nlm.nih.gov/compound/23985 (accessed 10.3.18).

National Center for Biotechnology Information, 2018b. Cupric oxide [WWW Document]. PubChem Compd. Database. URL https://pubchem.ncbi.nlm.nih.gov/compound/14829 (accessed 10.3.18).

Otanicar, T.P., Phelan, P.E., Golden, J.S., 2009. Optical properties of liquids for direct absorption solar thermal energy systems. Sol. Energy 83, 969–977. https://doi.org/10.1016/j.solener.2008.12.009.

Otanicar, T.P., Phelan, P.E., Prasher, R.S., Rosengarten, G., Taylor, R.A., 2010. Nanofluid-based direct absorption solar collector. J. Renew. Sustain. Energy 2, 033102. https://doi.org/10.1063/1.3429737.

Patel, J., Němcová, L., Maguire, P., Graham, W.G., Mariotti, D., 2013. Synthesis of surfactant-free electrostatically stabilized gold nanoparticles by plasma-induced liquid chemistry. Nanotechnology 24, 245604. https://doi.org/10.1088/0957-4484/24/24/245604.

Phelan, P., Otanicar, T., Taylor, R., Tyagi, H., 2013. Trends and opportunities in direct-absorption solar thermal collectors. J. Therm. Sci. Eng. Appl. 5, 1–9. https://doi.org/10.1115/1.4023930.

Pustovalov, V.K., Astafyeva, L.G., 2018. Optical properties of nanoparticles and nanofluids for direct absorption of solar radiation. Nanotechnol. Environ. Eng. 3, 1–8. https://doi.org/10.1007/s41204-018-0044-0.

Qu, J., Zhang, R., Wang, Z., Wang, Q., 2019. Photo-thermal conversion properties of

hybrid CuO-MWCNT/H2O nanofluids for direct solar thermal energy harvest. Appl. Therm. Eng. 147, 390–398. https://doi.org/10.1016/j.applthermaleng.2018.10.094.

Rose, B.A.J., Singh, H., Verma, N., Tassou, S., Suresh, S., Anantharaman, N., Mariotti, D., Maguire, P., 2017. Investigations into nanofluids as direct solar radiation collectors. Sol. Energy 147, 426–431. https://doi.org/10.1016/j.solener.2017.03.063.

Saidur, R., Meng, T.C., Said, Z., Hasanuzzaman, M., Kamyar, A., 2012. Evaluation of the effect of nanofluid-based absorbers on direct solar collector. Int. J. Heat Mass Transf. 55, 5899–5907. https://doi.org/10.1016/j.ijheatmasstransfer.2012.05.087.

Seinfeld, J., Pandis, S., 2006. Atmospheric Chemistry and Physics. John Wiley and Sons.

Sharaf, O.Z., Rizk, N., Joshi, C.P., Abi Jaoudé, M., Al-Khateeb, A.N., Kyritsis, D.C., Abu-Nada, E., Martin, M.N., 2019. Ultrastable plasmonic nanofluids in optimized direct absorption solar collectors. Energy Convers. Manag. 199, 112010. https://doi.org/10.1016/j.enconman.2019.112010.

Steinigeweg, D., Schütz, M., Salehi, M., Schlücker, S., 2011. Fast and Cost-Effective Purification of Gold Nanoparticles in the 20–250 nm Size Range by Continuous Density Gradient Centrifugation. Small n/a-n/a. https://doi.org/10.1002/smll.201100663.

Suchomel, P., Kvitek, L., Prucek, R., Panacek, A., Halder, A., Vajda, S., Zboril, R., 2018. Simple size-controlled synthesis of Au nanoparticles and their size-dependent catalytic activity. Sci. Rep. 8, 4589. https://doi.org/10.1038/s41598-018-22976-5.

Taylor, R.A., Phelan, P.E., Otanicar, T.P., Adrian, R., Prasher, R., 2011. Nanofluid optical property characterization: towards efficient direct absorption solar collectors. Nanoscale Res. Lett. 6, 225. https://doi.org/10.1186/1556-276X-6-225.

Turner, N.H., Single, A.M., 1990. Determination of peak positions and areas from wide-scan XPS spectra. Surf. Interface Anal. 15, 215–222. https://doi.org/10.1002/sia.740150305.

Tyagi, H., Phelan, P., Prasher, R., 2009. Predicted Efficiency of a Low-Temperature Nanofluid-Based Direct Absorption Solar Collector. J. Sol. Energy Eng. 131, 041004. https://doi.org/10.1115/1.3197562.

Ulset, E.T., Kosinski, P., Zabednova, Y., Zhdaneev, O.V., Struchalin, P.G., Balakin, B.V., 2018. Photothermal boiling in aqueous nanofluids. Nano Energy 50, 339–346. https://doi.org/10.1016/j.nanoen.2018.05.050.

Vakili, M., Hosseinalipour, S.M., Delfani, S., Khosrojerdi, S., Karami, M., 2016. Experimental investigation of graphene nanoplatelets nanofluid-based volumetric solar collector for domestic hot water systems. Sol. Energy 131, 119–130. https://doi.org/10.1016/j.solener.2016.02.034.

Velusamy, T., Liguori, A., Macias-Montero, M., Padmanaban, D.B., Carolan, D., Gherardi, M., Colombo, V., Maguire, P., Svrcek, V., Mariotti, D., 2017. Ultra-small CuO nanoparticles with tailored energy-band diagram synthesized by a hybrid plasma-liquid process. Plasma Process. Polym. 14, 1600224. https://doi.org/10.1002/ppap.201600224.

Verma, V.C., Singh, S.K., Solanki, R., Prakash, S., 2010. Biofabrication of Anisotropic Gold Nanotriangles Using Extract of Endophytic Aspergillus clavatus as a Dual Functional Reductant and Stabilizer. Lett. Nanoscale Res. https://doi.org/10.1007/s11671-010-9743-6.

Wang, X.-Q., Mujumdar, A.S., 2007. Heat transfer characteristics of nanofluids: a review. Int. J. Therm. Sci. 46, 1–19. https://doi.org/10.1016/j.ijthermalsci.2006.06.010.

Wang, Y., Lü, Y., Zhan, W., Xie, Z., Kuang, Q., Zheng, L., 2015. Synthesis of porous Cu 2 O/CuO cages using Cu-based metal–organic frameworks as templates and their gas-sensing properties. J. Mater. Chem. A 3, 12796–12803. https://doi.org/10.1039/C5TA01108F.